Mechanistic Insights into Stereoselective Catalysis—The Effects of Counterions in a Cu^{II}–Bissulfoximine-Catalyzed Diels–Alder Reaction

Carsten Bolm,[a] **Marc Martin,**[a] **Georg Gescheidt,**[b] **Cornelia Palivan,**[c]
Tsvetanka Stanoeva,[b] **Helmut Bertagnolli,**[d] **Martin Feth,**[d] **Arthur Schweiger,**[e, f]
George Mitrikas,[e] **and Jeffrey Harmer**[e]

Abstract: The initial steps of an enantioselective Diels–Alder reaction catalyzed by a Cu^{II}–bissulfoximine complex were followed by EXAFS (EXAFS = extended X-ray absorption fine structure), EPR (EPR = electron paramagnetic resonance) spectroscopy (CW-EPR, FID-detected EPR, pulse ENDOR, HYSCORE; CW = continuous wave; ENDOR = electron nuclear double resonance; HYSCORE = hyperfine sublevel correlation; FID = free induction decay), and UV-visible spectroscopy. The complexes formed between the parent CuX$_2$ (X = Cl$^-$, Br$^-$, TfO$^-$, SbF$_6^-$) salts, the chiral bissulfoximine ligand (S,S)-**1**, and N-(1-oxoprop-2-en-1-yl)oxazolidin-2-one (**2**) as the substrate in CH$_2$Cl$_2$ were investigated in frozen and fluid solution. In all cases, penta- or hexacoordinated Cu^{II} centers were established. The complexes with counterions indicating high stereoselectivity (TfO$^-$ and SbF$_6^-$) reveal one unique species in which substrate **2** binds to pseudoequatorial positions (via O atoms), shifting the counterions to axial locations. On the other hand, those lacking stereoselectivity (X = Cl$^-$ and Br$^-$) form two species in which the parent halogen anions remain at equatorial positions preventing the formation of geometries compatible with those found for X = TfO$^-$ and SbF$_6^-$.

Keywords: bissulfoximine complexes · catalysis · EPR spectroscopy · EXAFS spectroscopy · HYSCORE spectroscopy

Introduction

Enantioselective catalysis remains a highly competitive field in synthetic organic chemistry. A considerable number of ligands combined with various metal cations have been introduced as efficient catalysts for a broad variety of reaction types. A frequently utilized cation is Cu^{II}, which has been combined extensively with ligands containing nitrogen atoms that serve as potential binding sites, for example, bisoxazolines (BOX ligands),[1–3] phosphinooxazoline (PHOX),[4] or sulfoximine derivatives.[5–10] Lewis acid type catalysts of this type lead to high conversions and excellent selectivities in a vast array of reactions of the Grignard-type,[11] aldol condensations,[7,8,12] fluorinations,[13] and, prominently, Diels–Alder or hetero-Diels–Alder reactions.[5,6,14–17]

[a] Prof. Dr. C. Bolm, Dr. M. Martin
Institut für Organische Chemie der RWTH Aachen
Landoltweg 1, 52056 Aachen (Germany)
Fax: (+49) 241-809-2391
E-mail: Carsten.Bolm@oc.rwth-aachen.de

[b] Prof. Dr. G. Gescheidt, Dipl.-Chem. T. Stanoeva
Institute for Physical and Theoretical Chemistry
Graz University of Technology, Technikerstrasse 4/I
8010 Graz (Austria)
Fax: (+43) 316-873-8225
E-mail: gescheidt@ptc.tugraz.at

[c] Dr. C. Palivan
Department of Chemistry, University of Basel
Klingelbergstrasse 80, 4056 Basel (Switzerland)

[d] Prof. Dr. H. Bertagnolli, Dr. M. Feth
Institut für Physikalische Chemie der Universität Stuttgart
Pfaffenwaldring 55, 70569 Stuttgart (Germany)
Fax: (+49) 711-685-64443
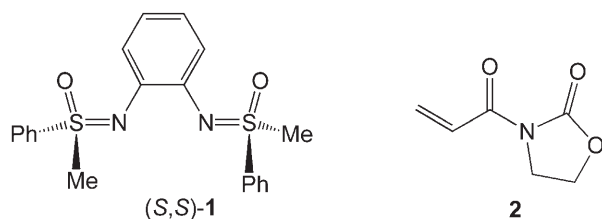E-mail: h.bertagnolli@ipc.uni-stuttgart.de

[e] Prof. Dr. A. Schweiger, Dr. G. Mitrikas, Dr. J. Harmer
Laboratory of Physical Chemistry
Department of Chemistry and Applied Biosciences
ETH-Zürich, 8093 Zürich (Switzerland)
Fax: (+41) 44-632-1021
E-mail: harmer@phys.chem.ethz.ch

[f] Prof. Dr. A. Schweiger
Deceased on January 4, 2006

Supporting information for this article contains the EXAFS of reference compounds dichloro(1,10-phenanthroline)copper(II) and dibromo(1,10-phenanthroline)copper(II) and EPR spectra of all complexes listed in Table 3 together with their simulations. These data are available on the WWW under http://www.chemeurj.org/ or from the author.

In various catalyses, it was found that the conversion and the enantioselectivity in asymmetric transition-metal catalysis were not exclusively governed by the structure of the chiral ligand, but also by the nature of the counterion in the parent metal salt.[5–8,17–22] Although this aspect has been discussed in several publications, the knowledge about the molecular background of these environmental effects is scarce. A recent theoretical investigation on Cu^I-catalyzed cyclopropanations using density functional theory[23a] illustrates how counterions substantially alter the structure of a catalyst and a review summarizes a vast palette of examples on ion-pairing effects in catalysis.[23b]

In a previous publication,[24] we have shown that the primary, decisive complex formed between Cu^{II} triflate and bissulfoximine (S,S)-**1** has a rather low symmetry and, most

Scheme 1. Example for a Diels–Alder reaction catalyzed by $[Cu^{II}\{(S,S)-\mathbf{1}\}(X_2)]$.

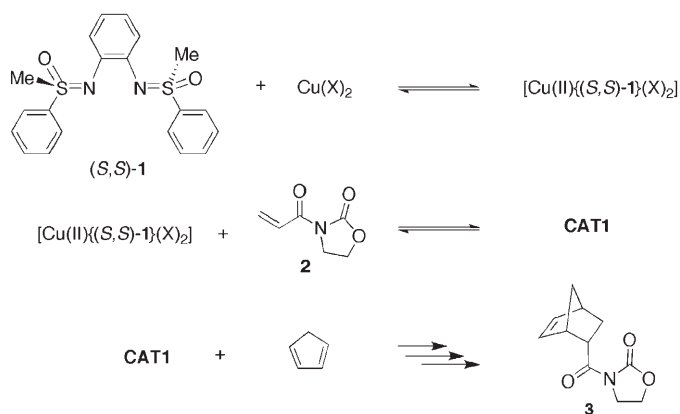likely, is very fluxional. Although the addition of a substrate molecule (N-(1-oxoprop-2-en-1-yl)oxazolidin-2-one, **2**) leads to a well-defined complex in one of the early steps of the catalytic reaction, its symmetry is low (distorted pyramidal).

A significant feature of the resulting complex is the presence of one axially positioned triflate (TfO^-) anion in the first coordination sphere of Cu^{II}. As the counterion can be expected to play a dominant role in the decisive steps of the catalysis, we have investigated how different counterions alter the geometry of this complex.

Here, we demonstrate how the counterions of the parent Cu^{II} salts (CuX_2) with $X = Cl^-$, Br^-, TfO^-, and SbF_6^- influence the stereoselectivity and how far this can be traced back to the structure of the primary complexes formed from CuX_2 and bissulfoximine **1**. The geometry of the complex $[Cu^{II}\{(S,S)-\mathbf{1}\}Br_2]$ is derived from EXAFS (EXAFS = extended X-ray absorption fine structure) measurements. Insights into the catalytic reaction in CH_2Cl_2 with the counterions Cl^-, Br^-, CF_3COO^-, and SbF_6^- is gained with the help of continuous wave (CW) and free induction decay detected (FID-detected) EPR (EPR = electron paramagnetic resonance), pulse electron nuclear double resonance (ENDOR), hyperfine sublevel correlation (HYSCORE), and optical spectroscopy.

Results

Observations from synthesis: Scheme 1 shows the typical reaction sequence for the catalyzed stereoselective Diels–Alder reaction using a copper salt CuX_2 ($X = TfO^-$, Br^-,

Cl^-, CF_3COO^-), bissulfoximine (S,S)-**1** as ligand, dienophile oxazolidin-2-one **2**, and cyclopentadiene. The reaction basically consists of three steps. In a first step, the catalyst $[Cu^{II}\{(S,S)-\mathbf{1}\}X_2]$ is formed. The next decisive stage yields, after reaction with dienophile **2**, the catalytically active complex **CAT1**. Finally, the diene is added leading to the desired Diels–Alder product **3**.

Although the anion X^- in the parent Cu^{II} salt virtually does not affect the overall conversion, the stereoselectivity, that is, the ee (ee = enamtiomeric excess) value is considerably influenced by the choice of the counterion (Table 1).[6]

Table 1. Influence of the counterions on the stereoselectivity of the reaction sequence displayed in Scheme 1 (taken from reference [6]).[a]

Entry	CuX_2	Conversion (%)	ee (%)[b]	endo/exo
1	$Cu(OTf)_2$	98	75	93:7
2	$CuCl_2$	98	0	93:7
3	$CuBr_2$[c]	98	0	93:7
4	$Cu(OOCCF_3)_2$	98	2	90:10
5	$Cu(SbF_6)_2$	98	73	93:7

[a] Reaction conditions: $Cu(X)_2$ (10 mol%), (S,S)-**1** (10 mol%), dienophile **2** (1 equiv), then cyclopentadiene (4 equiv), −70 °C, CH_2Cl_2. [b] Determined by HPLC using a chiral column (Chiralcel-OD). [c] See reference [46].

Whereas in the presence of TfO^- the ee value reaches 75%, it vanishes upon the use of $CuCl_2$ and $CuBr_2$, and hardly any enantioselectivity is observed with $Cu(OOCCF_3)_2$.

The reason for these dramatic deviations very likely has its origin in distinctly different structures of the catalytically active complex **CAT1**.

Solid-state XANES and EXAFS of complexes based on $CuBr_2$: According to EXAFS in the solid state, the solvent-free complex formed upon reaction of Cu^{II} triflate and (S,S)-**1** indicates a direct interaction between two oxygen atoms of the triflate anions and the two nitrogen atoms of ligand (S,S)-**1**. In CH_2Cl_2, this complex shows a high fluxionality in fluid solution and an asymmetric arrangement of the

ligands in frozen solution. The formation of higher aggregates in solution was ruled out in our initial investigation.[24]

The XANES (XANES = X-ray absorption near edge structure) spectra of the reaction products of (S,S)-**1** and CuBr₂ reflect distinctly different features than those with copper(II) triflate. Comparison of the copper K-edge XANES spectrum of CuBr₂ with the spectra of the reaction products of copper(II) bromide with one and two equivalents of (S,S)-**1** (Figure 1) shows that a reaction between the
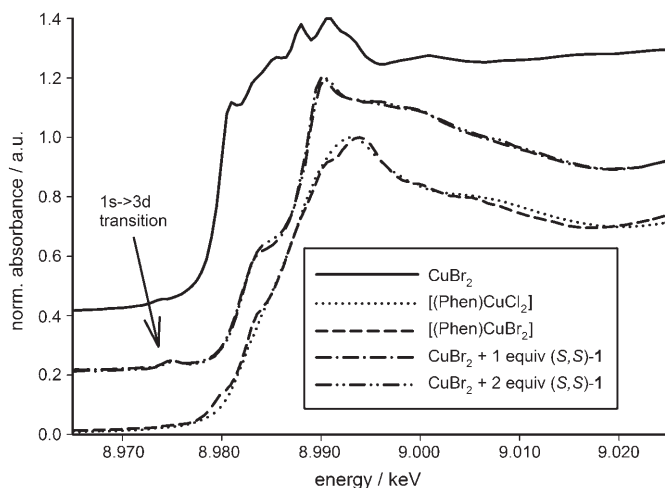

Figure 1. Comparison of the copper K-edge XANES regions of CuBr₂, [Cu(1,10-phenanthroline)Cl₂] (square-planar reference compound), [Cu(1,10-phenanthroline)Br₂] (square-planar reference compound), CuBr₂+one equivalent of (S,S)-1 (isolated from CH₂Cl₂) and CuBr₂+ two equivalents of (S,S)-1 (isolated from CH₂Cl₂). For details see the Supporting Information.

The 1s→3d transition feature has the highest intensity in pure tetrahedral complexes.[25] As the 1s→3d signal of the reaction product of CuBr₂ and (S,S)-**1** is significantly lower than in tetrahedral copper(II) complexes[25] a distorted square-planar geometry around the central copper atom in the reaction product is more likely.

A Cu–Br distance of 233 pm for [Cu{(S,S)-**1**}Br₂] was determined from both the Cu K- and the Br K-edge (Table 2). Remarkably, this distance is shorter than that of "free" CuBr₂ (240 pm). This strong interaction between the Cu^{II} cation and the Br⁻ anions is additionally illustrated by the observation that an excess of (S,S)-**1** does not lead to the formation of a cationic complex containing two bissulfoximine ligands. This is apparent from the almost identical EXAFS functions and copper K-edge XANES spectra (Figures 1 and 2) detected from the samples CuBr₂+one equivalent of (S,S)-**1** and CuBr₂+two equivalents of (S,S)-**1** (Table 2). The formation of higher associates cannot be established by EXAFS spectroscopy because it is virtually impossible to detect Cu–Cu distances larger than 350 pm.

Are the interactions of the central Cu^{II} and its nearest neighbors altered in the presence of the solvent? This has been investigated by various paramagnetic-resonance measurements.

CW-EPR, HYSCORE, and Davies ENDOR Spectroscopy: When ligand (S,S)-**1** is added to Cu(OTf)₂, CuCl₂, CuBr₂, and CuCl₂/AgSbF₆ (1:1) in CH₂Cl₂, the CW-EPR spectra attributed to [Cu^{II}{(S,S)-**1**}X₂] (Figure 3) were detected. As we have already noted in the previous publication, the EPR spectra slightly change their shape depending on the orientation of the samples with respect to the magnetic field. This

metal salt and the ligand has taken place. Both spectra with one and two equivalents of the ligand **1** are practically identical. This indicates that an excess of **1** does not lead to a rearrangement of the coordination sphere. In contrast to Cu-(OTf)₂, in both XANES spectra a prepeak signal at about 8974 eV can be detected and identified as a dipole allowed 1s→3d electron transition.[25] Sano et al. showed that tetrahedral and distorted square-planar copper(II) complexes exhibit a 1s→3d electron transition, whereas square-planar

Table 2. Structural parameters of CuBr₂ and the reaction products with one and two equivalents of bissulfoximine (S,S)-**1**. The data were determined from simulations of the experimental $k^3\chi(k)$ function (Cu K- and Br K-edges).[a]

	A–Bs	r [pm]	N	σ [pm]	E_0 [eV]	ΔE_0 [eV]	k range [Å⁻¹]	Fit index (R)
CuBr₂	Cu–Br	240	4.0	6.9	8987.5	16.8	3.40–16.00	32.8
	Br–Cu	240	1.0	6.0	13470.0	17.3	4.00–15.00	26.8
CuBr₂ + (S,S)-**1** (1 equiv)	Cu–N	201	2.1	6.0	8987.5	22.3	3.26–13.48	25.8
	Cu–Br	233	2.0	7.0				
	Cu–C	288	2.4	6.7				
	Cu–S	317	2.0	9.8				
	Br–Cu	233	1.1	6.9	13470.0	16.0	4.00–16.00	26.8
CuBr₂ + (S,S)-**1** (2 equiv)	Cu–N	201	1.9	7.7	8987.5	21.7	3.21–12.48	21.7
	Cu–Br	233	2.0	7.1				
	Cu–C	287	2.5	5.0				
	Cu–S	319	1.8	7.7				
	Br–Cu	233	1.1	6.8	13470.0	16.3	4.00–13.00	38.5

[a] Absorber A, backscatterer Bs, distance r, coordination number N, Debye–Waller factor σ with the calculated deviation, edge energy E_0, shift of the threshold energy ΔE_0 and fit index R.

complexes do not have this pre-edge feature. The last statement is illustrated by the XANES spectra of the square-planar reference compounds dichloro(1,10-phenanthroline)-copper(II)[26] and dibromo(1,10-phenanthroline)copper(II)[27] (Figure 1), in which no 1s→3d transition can be detected.

is due to the formation of microcrystallites by the solvent CH₂Cl₂, as it does not form a perfect glass. Therefore the experimental spectra do not represent perfectly averaged powder patterns. Accordingly, approximately eight orientations of the sample with respect to the magnetic field were
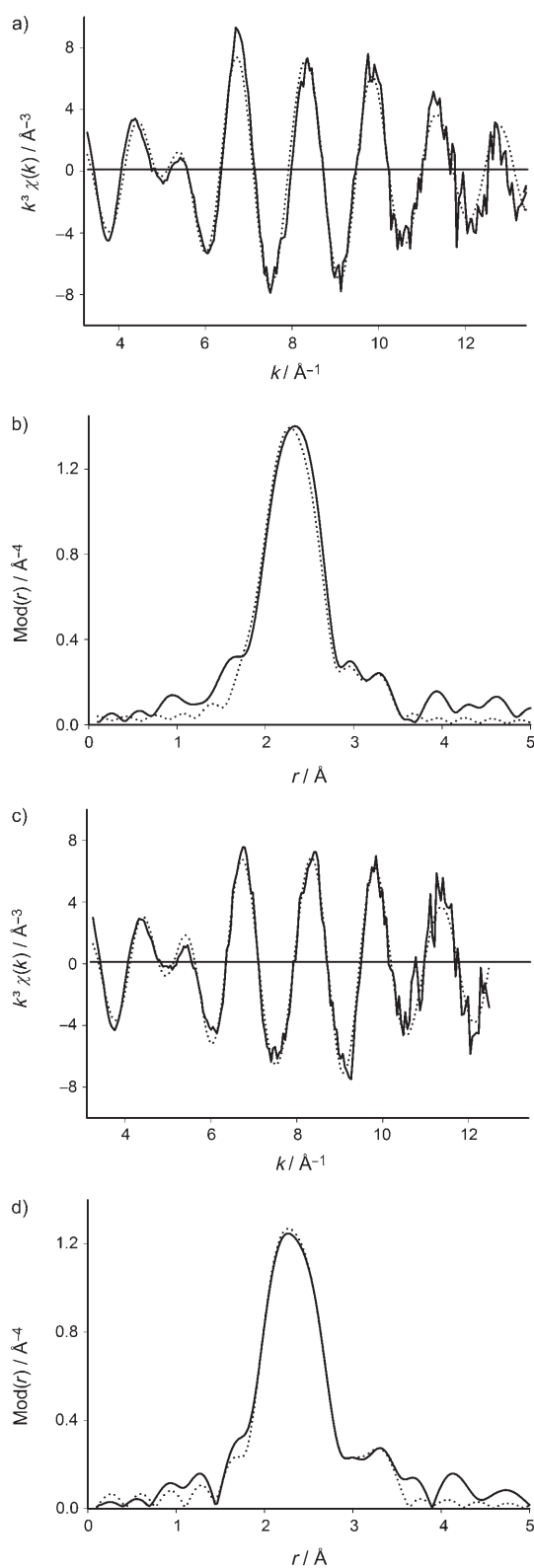
FULL PAPER

Figure 2. Experimental (solid line) and calculated (dotted line) $k^3\chi(k)$ functions (a), (c), and their Fourier transforms (b), (d) of solid $CuBr_2 +$ one equivalent of (S,S)-**1** and $CuBr_2 +$ two equivalents of (S,S)-**1** (isolated from CH_2Cl_2) at the Cu K-edge.
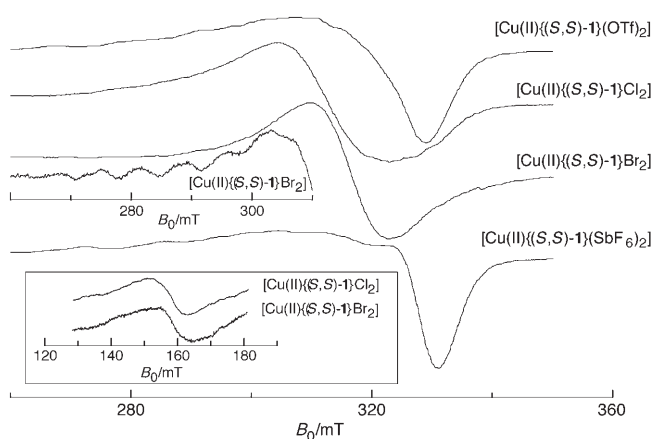

Figure 3. CW-EPR spectra of mixtures of (S,S)-**1** with $Cu(OTf)_2$, $CuCl_2$, $CuBr_2$, and $CuCl_2/AgSbF_6$ (1:1) in CH_2Cl_2 at 77 K. The inset shows the $\Delta M_S = \pm 2$ transitions at half field for $[Cu^{II}\{(S,S)$-**1**\}Cl_2]$ and $[Cu^{II}\{(S,S)$-**1**\}Br_2]$ (around 160 mT), the insert below the spectrum of $[Cu^{II}\{(S,S)$-**1**\}Br_2]$ shows its second derivative in the parallel region. Microwave frequencies: 9.4407 (TfO^-), 9.4350 (Cl^-,Br^-), 9.4349 ($SbCl_6^-$).

used to construct the spectra shown in Figure 3 (and Figure 4). It is noteworthy that this orientational dependence of the EPR signals does not affect the EPR parameters.

The spectra of $[Cu^{II}\{(S,S)$-**1**\}X_2]$ with $X = TfO^-$ and $X = SbF_6^-$ are rather similar with resolved copper hyperfine splittings along g_z. Both spectra could be simulated with a single Cu^{II} species (Table 3). On the other hand, spectra with $X = Cl^-$, Br^- show an almost isotropic shape, but instead of the four lines expected for $^{63,65}Cu$ in the parallel region, six lines are visible (for $[Cu^{II}\{(S,S)$-**1**\}Br_2]$ see insert at the bottom of Figure 3). Their overall spectrum shape did not change by decreasing the sample concentration from 5.2 to 0.8 mM. Moreover, half-field transitions (at 160 mT) are observable at low temperatures, indicating spin–spin interactions (for example, an interaction between two unpaired electrons).

To distinguish between the different components in the spectra with Cl^- and Br^- counterions, FID-detected EPR spectra were taken by recording the signal following a single microwave pulse. This method can be used as a filter as it is sensitive to the decay time of the transverse magnetization, T_m. In the current experiments, the FID signals were recorded for times being greater than 100 ns after the mw (mw = microwave) pulse (the spectrometer deadtime is $t_d = 100$ ns). Representative spectra are given in Figure 4 for $[Cu^{II}\{(S,S)$-**1**\}Cl_2]$, which displays both the FID-detected EPR and CW-EPR spectra, and their simulations (a complete set of simulations is shown in the Supporting Information). The FID-detected and CW-EPR spectra are clearly different, showing two distinctly different species, one with a long phase memory time $T_m \gg t_d$ seen in the FID-detected spectrum, and one with a short phase memory time $T_m < t_d$ that is additionally observed in the CW-EPR spectrum. The FID-detected spectrum could be simulated with a single Cu^{II} species (Table 3). The simulation of the CW-EPR spectrum re-

Table 3. EPR parameters for the initial two steps of the catalytic reaction, (S,S)-**1**+CuX_2 and (S,S)-**1**+CuX_2+**2**. In the case for which $X = Cl^-$ or Br^- a two-component model was used, whereas with $X = TfO^-$ or SbF_6^- a single Cu^{II} species was sufficient to simulate the EPR spectra. For the experimental spectra and their simulations see the Supporting Information.

Sample	Spectral composition[b]	g_x	g_y	g_z	A_x[c]	A_y[c]	A_z[c]	D[d]	$L_{x,y}$[e]	L_z[e]
(S,S)-**1**+$CuCl_2$	25	2.047	2.105	2.355	<40	<40	210	–	180	250
	75		2.12	2.27	–	–	–	312	400	600
(S,S)-**1**+$CuCl_2$+**2**	75	2.060	2.115	2.360	<60	<20	220	–	200	200
	25		2.12	2.26	–	–	–	312	300	700
(S,S)-**1**+$CuBr_2$	<15	2.06	2.16	2.39	<60	<60	320	–	300	350
	>85		2.12	2.18	–	–	–	240	400	600
(S,S)-**1**+$CuBr_2$+**2**	<40	2.05	2.16	2.39	<60	<60	320	–	350	450
	>60		2.10	2.20	–	–	–	312	400	700
(S,S)-**1**+$CuCl_2$+$2AgSbF_6$			2.075	2.293	102	102	347	–	200	200
(S,S)-**1**+$CuCl_2$+$2AgSbF_6$+**2**			2.068	2.332	29	29	418	–	200	200
(S,S)-**1**+$Cu(OTf)_2$+**2**[a]			2.068	2.357	23	23	409	-	200	200

[a] Result published previously, see reference [24]. [b] In %; error ≈15%. [c] Hyperfine couplings (absolute value) in MHz. [d] Electron–electron dipolar coupling for an axial interaction $(-D, -D, 2D)$ MHz. [e] Line width in MHz.
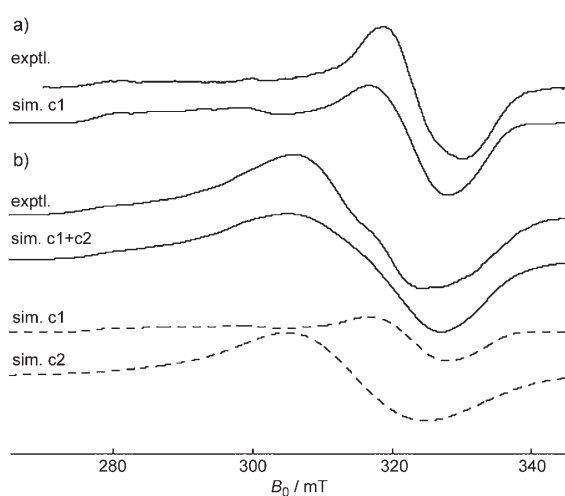

Figure 4. EPR spectra of (S,S)-**1**+$CuCl_2$ in the $g = 2$ region. a) FID-detected EPR spectrum and simulation (c1). b) CW-EPR spectrum and simulations which comprise the FID-detected EPR spectrum (c1: 25%) and a quasi-isotropic component (c2: 75%) that is associated with the half-field signal (microwave frequency for experimental spectra: 9.4920 GHz).

Figure 5. EPR spectra of $[Cu^{II}\{(S,S)$-**1**$\}X_2]$ after addition of **2**, in CH_2Cl_2 at 77 K. $X = TfO^-$, Cl^-, Br^-, and SbF_6^-. Microwave frequency: 9.4358, 9.4356, 9.4461, 9.4390 GHz, respectively.

quired a second quasi-isotropic component, which is associated with the half-field transitions. The spin-Hamiltonian used to simulate the latter species thus includes a spin–spin interaction D. Similarly for the sample $[Cu^{II}\{(S,S)$-**1**$\}Br_2]$, a two component model was required to simulate the FID-detected and CW-EPR spectra. The EPR parameters are given in Table 3.

When substrate **2** is reacted with $[Cu^{II}\{(S,S)$-**1**$\}X_2]$, a distinct behavior for the different counterions is observed. With TfO^- and SbF_6^-, almost identical EPR spectra are observed (Figure 5) which are significantly better resolved than their precursors and very similar to the complex (S,S)-**1**+$Cu(OTf)_2$+**2** previously investigated.[24] These two samples could be well simulated with single Cu^{II} complexes that have very similar EPR parameters, which we ascribe to complex **CAT1** (Scheme 1).
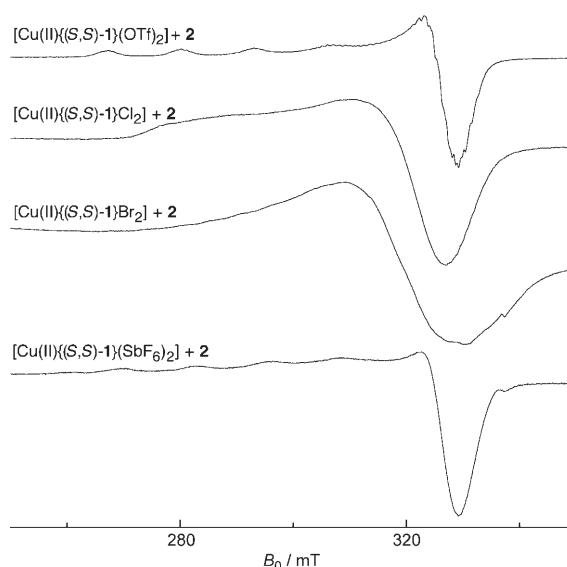
By starting with $CuCl_2$ and $CuBr_2$, different results were obtained, which were again investigated by FID-detected EPR and CW-EPR measurements. The FID-detected spectra in the case of both Cl^- and Br^- were similar before and after addition of substrate **2**, a result which is reflected in the g and copper hyperfine values (A_i) given in Table 3. The CW-EPR spectra could be simulated with a two-component model consisting of the Cu^{II} complex found in the FID-detected EPR spectrum, and an additional broad quasi-isotropic component with an associated half-field signal. Comparing the spectra before and after addition of **2** shows that the percentage of the quasi-isotropic component is reduced. This analysis is in qualitative agreement with the FID intensity which increased upon addition of **2** for both Cl^- and Br^- samples, even though the sample concentration was the same (approximately 5 mM).

The quasi-isotropic signals containing either Cl⁻ or Br⁻ counterions before and after addition of **2** have very short phase memory times and show half-field signals, pointing towards the formation of dimeric Cu^II complexes in the solid state. The lack of any discernable copper hyperfine structure in these signals is probably the result of a considerable isotropic exchange interaction. The intensity ratio between the $\Delta M_S = \pm 1$ and $\Delta M_S = \pm 2$ transitions can be used to estimate the Cu^II–Cu^II distances:[28] approximately 550 pm for [Cu^II-{(S,S)-**1**}Cl_2] and [Cu^II{(S,S)-**1**}Cl_2+**2**], approximately 600 pm for [Cu^II{(S,S)-**1**}Br_2], and approximately 550 pm for [Cu^II-{(S,S)-**1**}Br_2+**2**]. As these values are determined from the signal intensity ratio between the anisotropic component in the $g=2$ region and the half-field transition, they carry rather significant errors (approximately 20%). Spin–spin interactions between copper ions can be mediated by halide bridging and give rise either to dimeric or to polymeric Cu^II⋯halogenide arrangements in crystallized complexes. In such crystals, bis-halide dimers have a Cu–Cu distance in the order of 340–440 pm,[29–31] in polymeric chains these distances become larger depending on the type of bridging. For bisbridged halide copper compounds this value is around 450 pm,[32] for monobridged halide chains it is larger than 470 pm.[33,34] In polymeric chains, an apical Cu–halide interaction exists among the repeating units, in which the axial Cu–halide bonds are longer than the equatorial ones. The monohalide bridged Cu chains are usually found when the ligand induces steric constraints, which prevent a symmetric bisbridging arrangement. If in stackings the ligands are not exactly in alternate orientations, the formation of only one halogen bridge, giving rise to a zig-zag chain, is favored.[34]

Remarkably, the distances of ≈600 pm between two Cu^II cations estimated by the analysis of the CW-EPR spectra of the frozen CH_2Cl_2 solutions of [Cu^II{(S,S)-**1**}Cl_2] and [Cu^II-{(S,S)-**1**}Br_2] greatly exceed the corresponding distances in the (solvent-free) crystallized complexes discussed above. They are also significantly longer than twice the Cu–Br distances determined for the solvent-free complexes by EXAFS (466 pm for [Cu^II{(S,S)-**1**}Br_2], Table 2) These exceedingly long Cu^II–Cu^II distances can be provisionally explained with the presence of monobridging halogen anions in axial positions. As this feature is exclusively observed for the Cu^II complexes in the presence of CH_2Cl_2 it can be anticipated that the chlorine atoms of the solvent participate in the Cu^II–Cu^II interaction. Moreover, the long distance can be traced back to the steric demand of the bulky ligand (S,S)-**1**. It is, however, tentative as to whether these features are of relevance for the catalytic reaction as they are exclusively detectable in frozen solution.

To get more insight into the coordination sphere of the species containing Cl⁻ and Br⁻ counterions, pulse EPR measurements were performed. These pulse experiments, like the FID-detected EPR measurements, are sensitive to the T_m time and thus signals come only from the complexes giving rise to FID-detected EPR spectra, which, very likely, represent the species also present in fluid solution. Representative Davies-ENDOR and HYSCORE experiments at

X-band on the sample with [Cu^II{(S,S)-**1**}Cl_2] before and after addition of **2** are shown in Figures 6 and 7, respectively. The Davies-ENDOR spectra were recorded with both long and short π inversion microwave (mw) pulses, the former being most sensitive to small couplings and the latter to large couplings. With short pulses, the spectra contain broad signals which indicate the presence of strongly coupled ^14N
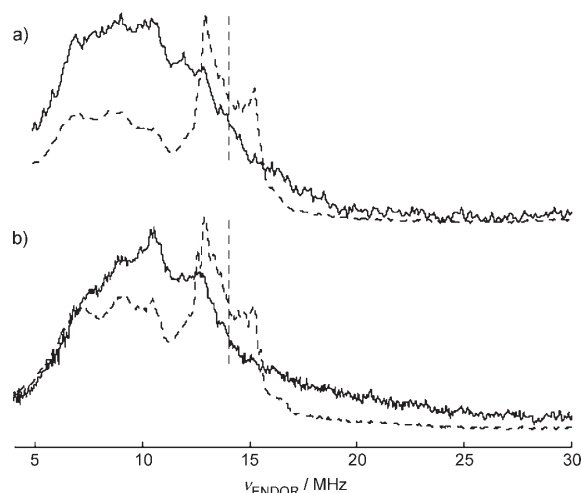

Figure 6. X-band (9.7 GHz) Davies-ENDOR spectra at an observer position between $g_{x,y}$ and g_z ($B_0 = 330$ mT) of the species containing a) [Cu^II-{(S,S)-**1**}Cl_2] and b) [Cu^II{(S,S)-**1**}Cl_2+**2**]. Dashed and solid lines were recorded with a 200 and 32 ns inversion mw π pulse, respectively. The horizontal line shows the proton Larmor frequency.
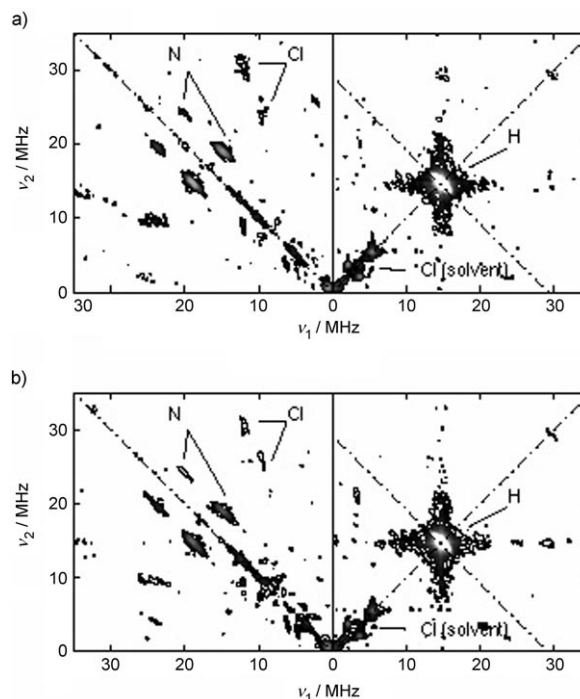

Figure 7. X-band (9.7 GHz) HYSCORE spectra at an observer position near g_x ($B_0 = 343$ mT) of the species containing a) [Cu^II{(S,S)-**1**}Cl_2], and b) [Cu^II{(S,S)-**1**}Cl_2+**2**].

and/or ^{35,37}Cl nuclei (with hyperfine couplings of $|A| \approx 8$–32 MHz. In addition, signals from weakly coupled protons ($|A| < 5$ MHz), assigned to the (S,S)-**1**, are observed (most pronounced with long mw pulses). Signals from the samples before and after addition of **2** are very similar, an indication that the equatorial Cl⁻ ligands have not been replaced. A similar conclusion can be drawn from the X-band HYS-CORE spectra shown in Figure 7. In both spectra, peaks attributable to ^{14}N nuclei are labeled, with hyperfine couplings in the range $|A(^{14}N)| \approx 14$–29 MHz (split by approximately twice the Larmor frequency of ^{14}N). The cross-peaks around (−28,6) MHz and (−6,28) MHz are tentatively assigned to Cl nuclei, with hyperfine couplings in the range 15–29 MHz. This range of ^{14}N and ^{35,37}Cl hyperfine couplings is consistent with the broad signals observed in the ENDOR spectra. The low-frequency peaks in the X-band HYSCORE spectra can be assigned to ^{35,37}Cl from the solvent, with small hyperfine coupling constants $|A(Cl)| \approx 2$ MHz.

In summary, the measurements reveal two species for the samples containing either Cl⁻ or Br⁻ counter ions. The quasi-isotropic components (only visible in the CW-EPR spectrum) result from Cu^{II}–Cu^{II} interactions and point to the formation of "associated" Cu complexes in the solid state. The complexes exclusively observed in the FID-detected spectra are similar before and after addition of **2** in the case of either Cl⁻ or Br⁻ counterions. ENDOR and HYSCORE spectra are also similar for the strongly coupled nuclei and reveal low symmetry (orthorhombic tensors, see Table 3). This suggests that in the FID-detected species observed both before and after addition of **2**, the Cu^{II} is equatorially coordinated by the two nitrogens of (S,S)-**1** and the counterions Cl⁻ or Br⁻. The change upon addition of substrate **2** for both Cl⁻ and Br⁻ samples probably results from an exchange of a weakly coordinating pseudoaxial ligand, which could be a Cl atom from the solvent CH$_2$Cl$_2$ before **2** is added. After its addition, the oxygen atoms of **2** are most likely to be involved.

Electronic absorption spectra: The characterization of these complexes in solution at room temperature is complemented by UV-visible spectroscopy. The low symmetry of the species before the addition of the substrate is indicated by the position of the d–d bands in electronic spectra (around 704 nm for Cl⁻ and 792 nm for Br⁻).[36,37] After the addition of the substrate in both cases, the intensity of the d–d bands increases. This enhancement is specific for a more distorted geometry around the metal as the d–d transitions become allowed as electric dipole transitions.[38]

The electronic spectra in solution at room temperature, therefore, support the change of the geometry simultaneously with the decrease of the copper coordination number when the substrate is added.

None of the EPR or electronic spectra for Br⁻ and Cl⁻ are similar to those obtained in the case of TfO⁻ and SbF$_6$⁻. All together, our results demonstrate that in the case of Cl⁻ and Br⁻ as counterions, the substrate **2** does not replace

them to form **CAT1** (Scheme 1), in contrast to TfO⁻ and SbF$_6$⁻.

Conclusions

In the case of TfO⁻ or SbF$_6$⁻ as the counterions, a complex is formed, which involves an asymmetric coordination sphere around Cu^{II} involving ligand (S,S)-**1** (binding via two nonequivalent nitrogen atoms), substrate **2** which replaces two equatorially bound counterions (bound via two nonequivalent oxygen atoms), and weakly bound counterions in an axial position.[24] A different situation exists for Cl⁻ and Br⁻ as the counterions. Two distinct complexes are established: one, [Cu^{II}{(S,S)-**1**}X$_2$] (X = Cl⁻, Br⁻) reveals Cu^{II}–Cu^{II} electron–electron spin interactions via axial halogen atoms in the solid state. Upon addition of the substrate **2**, this arrangement is disturbed in terms of a change towards a significantly distorted arrangement with strongly tetracoordinated Cl⁻ (and Br⁻) anions and N atoms of (S,S)-**1**, with the two oxygen atoms of **2** only being able to replace the weakly bound pseudoaxial halogen atoms (Figure 8). The finding that addition of **2** leads to a decrease of the CW-
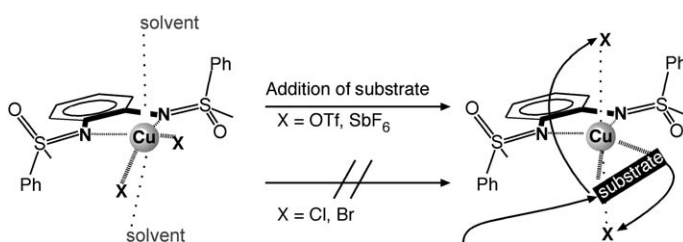
Figure 8. Schematic representation of substrate addition and alterations of the ligand sphere of [Cu^{II}{(S,S)-**1**}X$_2$].

EPR signal representing the species with a Cu^{II}–Cu^{II} interaction underpins that the two O atoms of this substrate are only able to replace axially bound halogen atoms (which are responsible for the electron–electron interaction between the two Cu^{II} cations).

Remarkably, in the cases in which a good stereoselectivity is observed, unique (well-defined) Cu^{II} complexes are formed, as established by EPR measurements.[24] However, in the case of Cl⁻ and Br⁻ as the counterions, two distinctly different complexes are discernible. Moreover, our results suggest that stereoselectivity requires weakly coordinating counterions, which are able to move to axial positions during the catalytic cycle, thus allowing the substrate(s) to occupy equatorial positions. This has also been observed for other types of catalytic systems.[39] Further investigations are necessary to establish if this is a general requirement for homogeneous enantioselective catalysis.

FULL PAPER

Experimental Section

EXAFS: Parent $Cu^{II}Br_2$ and bissulfoximine (*S,S*)-**1** were dissolved in CH_2Cl_2 (molar ratio 1:1 and 1:2). After the mixture of the components became homogeneous, the solvent was evaporated in vacuo. Dichloro(1,10-phenanthroline)copper(II) and dibromo(1,10-phenanthroline)copper(II) were purchased by Sigma-Aldrich and used as obtained.

The EXAFS measurements were performed at beamline X1.1 (RÖMO II) at the Hamburger Synchrotronstrahlungslabor des Deutschen Elektronensynchrotrons (HASYLAB at DESY, Hamburg, Germany) and at beamline KMC-2 at the Berliner Elektronenspeicherring-Gesellschaft für Synchrotronstrahlung m.b.H (BESSY II, Berlin, Germany). For the measurements at the Cu K- (8979.0 eV) and Br K-edge (13474.0 eV) a Si-(111) and a Si(311) double crystal monochromator was used at HASYLAB. At BESSY, a Si(220) double-graded crystal (0.5% Ge cm^{-1}) monochromator was used for the copper and bromine edges. The tilt of the second monochromator crystal was set to 40% harmonic rejection. Energy resolution was estimated to be about 0.7–1.0 eV at the Cu K-edge. Energy calibration was performed with the corresponding metal foil. The synchrotron beam current was between 80–100 mA at HASYLAB (positron energy 4.45 GeV) and between 100–250 mA at BESSY (electron energy 1.7 GeV).

All experiments were carried out under ambient conditions in transmission mode with ion chambers at 25 °C. All ion chambers were filled with nitrogen in the case of the measurements at the Cu K-edge and the second and third chamber with argon in the case of the measurements at the Br K-edge. Energy calibration was performed with copper metal foil in the case of measurements at the copper K-edge and lead metal foil (Pb L$_{III}$-edge) in the case of the bromine K-edge. The solid samples were embedded in a polyethylene matrix and pressed to pellets. The concentration of all samples was adjusted to yield an absorption jump of $\Delta\mu d \approx 1.5$.

Data evaluation started with background absorption removal from the experimental absorption spectrum by subtraction of a Victoreen-type polynomial. Then the background subtracted spectrum was convoluted with a series of increasingly broader Gauss functions and the common intersection point of the convoluted spectra was taken as energy E_0.[40,41] To determine the smooth part of the spectrum, corrected for pre-edge absorption, a piecewise polynomial was used. It was adjusted in such a way that the low-R components of the resulting Fourier transform were minimal. After division of the background-subtracted spectrum by its smooth part, the photon energy was converted to photoelectron wave numbers k. The resulting EXAFS function was weighted with k^3. Data analysis in k space was performed according to the curved wave multiple scattering formalism of the program EXCURV92 with XALPHA-phase and amplitude functions.[42] The mean free path of the scattered electrons was calculated from the imaginary part of the potential (VPI was set to -4.00) and an overall energy shift (ΔE_0) was assumed. The Amplitude reduction factor (AFAC) was set to a value of 0.8.

EPR: In dry CH_2Cl_2, equimolar amounts of the CuX$_2$ salts (X = Cl$^-$, Br$^-$, TfO$^-$, SbCl$_6^-$) were suspended under nitrogen. Then the ligand (*S,S*)-**1** was added (10 mg, 1:1 molar ratio versus the Cu^{II} salt). The solution was kept under nitrogen and stirred for approximately 30 minutes until the complex [Cu^{II}{(*S,S*)-**1**}(X)$_2$] was formed. Then **2** was added in five-fold molar excess to [Cu^{II}{(*S,S*)-**1**}(X)$_2$] under nitrogen. This solution was transferred into the EPR sample tube under inert gas. The sample was then degassed by three freeze-pump-thaw cycles under high vacuum and sealed. Five samples were prepared by this procedure and gave identical EPR spectra.

CW-EPR measurements were performed on a Bruker ESP300 X-band spectrometer equipped with a rectangular TE$_{102}$ cavity and on a Bruker E500 spectrometer equipped with a super-high Q cavity. For the measurements at 77 K, the sample was inserted in a Dewar filled with liquid nitrogen. During the EPR measurements in fluid solution in situ UV-visible spectra were taken on a diode-array fiber-optics spectrometer (J&M, Aalen, Germany).[43]

Pulse experiments at X-band were carried out on a Bruker E580 spectrometer (mw frequency 9.68 GHz) at 8–20 K. Davies-ENDOR experiments at X-band were carried out with the pulse sequence π–T–$\pi/2$–τ–π–τ–echo. One sequence employed a π ($\pi/2$) pulse of length 200 (100) ns and the second sequence employed a π ($\pi/2$) pulse of length 32 (16) ns (hyperfine contrast selectivity to suppress the spectral features of weakly coupled protons). A radio frequency pulse with a length of 9 μs was used. The field-swept EPR spectra were recorded by integrating the signal intensity of the FID following a mw pulse of length 800 ns. The HYSCORE experiments were carried out by using the pulse sequence $\pi/2$–τ–$\pi/2$–t_1–π–t_2–$\pi/2$–τ–echo with mw pulses of length $t_{\pi/2}=t_\pi=16$ ns, a τ value of 158 ns, a starting time of 96 ns for t_1 and t_2, and a time increment $\Delta t = 12$ ns (data matrix 350×350); an eight-step phase cycle was used.

EPR spectra were simulated by using Easyspin[44] and SimFonia[45] software based on a third-order perturbation theory treatment with the assumption that gyromagnetic and hyperfine tensors are aligned. Linewidth tensors were based on Lorentzian (295 K) and Gaussian (77 K) shape.

The ^{63}Cu/^{65}Cu isotopes in their natural abundance were considered for each spectrum. The simulations were performed until further changes in the EPR parameters did not improve the quality of the fit.

Acknowledgements

[1] D. A. Evans, J. S. Johnson in *Comprehensive Asymmetric Catalysis, Vol. 3* (Eds.: E. N. Jacobsen, A. Pfaltz, H. Yamamoto), Springer-Verlag, Berlin, **1999**, pp. 1177.

[2] D. A. Evans, M. C. Kozlowski, J. A. Murry, C. S. Burgey, K. R. Campos, B. T. Connell, R. J. Staples, *J. Am. Chem. Soc.* **1999**, *121*, 669.

[3] J. S. Johnson, D. A. Evans, *Acc. Chem. Res.* **2000**, *33*, 325.

[4] a) A. Pfaltz, *Chimia* **2001**, *55*, 708; b) G. Helmchen, A. Pfaltz, *Acc. Chem. Res.* **2000**, *33*, 336.

[5] a) C. Bolm, O. Simic, *J. Am. Chem. Soc.* **2001**, *123*, 3830; b) C. Bolm, M. Verrucci, O. Simic, C. P. R. Hackenberger, *Adv. Synth. Catal.* **2005**, *347*, 1696.

[6] C. Bolm, M. Martin, O. Simic, M. Verrucci, *Org. Lett.* **2003**, *5*, 427.

[7] a) M. Langner, C. Bolm, *Angew. Chem.* **2004**, *116*, 6110; *Angew. Chem. Int. Ed.* **2004**, *43*, 5984; b) M. Langner, P. Rémy, C. Bolm, *Chem. Eur. J.* **2005**, *11*, 6254.

[8] P. Rémy, M. Langner, C. Bolm, *Org. Lett.* **2006**, *8*, 1209.

[9] M. Langner, P. Rémy, C. Bolm, *Synlett* **2005**, 781.

[10] Recent reviews: a) H. Okamura, C. Bolm, *Chem. Lett.* **2004**, *33*, 482; b) M. Harmata, *Chemtracts* **2003**, *16*, 660; c) M. Reggelin, C. Zur, *Synthesis* **2000**, 1.

[11] B. L. Feringa, R. Badorrey, D. Pena, S. R. Harutyunyan, A. J. Minnaard, *Proc. Natl. Acad. Sci. USA* **2004**, *101*, 5834.

[12] S. Orlandi, M. Benaglia, F. Cozzi, *Tetrahedron Lett.* **2004**, *45*, 1747.

[13] J.-A. Ma, D. Cahard, *Tetrahedron: Asymmetry* **2004**, *15*, 1007.

[14] A. Bayer, M. M. Endeshaw, O. R. Gautun, *J. Org. Chem.* **2004**, *69*, 7198.

[15] K. A. Jørgensen, *Eur. J. Org. Chem.* **2004**, 2093.

[16] M. P. Sibi, H. Matsunaga, *Tetrahedron Lett.* **2004**, *45*, 5925.

[17] C. Bolm, M. Verrucci, O. Simic, P. G. Cozzi, G. Raabe, H. Okamura, *Chem. Commun.* **2003**, 2826.

[18] J. Thorhauge, M. Roberson, R. G. Hazell, K. A. Jørgensen, *Chem. Eur. J.* **2002**, *8*, 1888.

[19] M. J. Fernandez, J. M. Fraile, J. I. Garcia, J. A. Mayoral, M. I. Burguete, E. Garcia-Verdugo, S. V. Luis, M. A. Harmer, *Top. Catal.* **2000**, *13*, 303.

[20] D. G. Blackmond, A. Lightfoot, A. Pfaltz, T. Rosner, P. Schnider, N. Zimmermann, *Chirality* **2000**, *12*, 442.

[21] M. Johannsen, K. A. Jørgensen, *J. Chem. Soc. Perkin Trans. 2* **1997**, 1183.

[22] D. A. Evans, J. A. Murry, P. von Matt, R. D. Norcross, S. J. Miller, *Angew. Chem.* **1995**, *107*, 864; *Angew. Chem. Int. Ed. Engl.* **1995**, *34*, 798.

[23] a) J. M. Fraile, J. I. Garcia, M. J. Gil, V. Martinez-Merino, J. A. Mayoral, L. Salvatella, *Chem. Eur. J.* **2004**, *10*, 758; b) A. Macchioni, *Chem. Rev.* **2005**, *105*, 2039.

[24] C. Bolm, M. Martin, G. Gescheidt, C. Palivan, D. Neshchadin, H. Bertagnolli, M. Feth, A. Schweiger, G. Mitrikas, J. Harmer, *J. Am. Chem. Soc.* **2003**, *125*, 6222.

[25] M. Sano, S. Komorita, H. Yamatera, *Inorg. Chem.* **1992**, *31*, 459.

[26] D. Boys, C. Escobar, S. Martinez-Carrera, *Acta Crystallogr. Sect. B* **1981**, *37*, 351.

[27] M. T. Garland, D. Grandjean, E. Spodine, A. M. Atria, J. Manzur, *Acta Crystallogr. Sect. C* **1988**, *44*, 1547.

[28] S. S. Eaton, K. M. More, B. M. Sawant, G. R. Eaton, *J. Am. Chem. Soc.* **1983**, *105*, 6560.

[29] X. R. Bu, C. R. Jackson, D. Van Derveer, X. Z. You, Q. J. Meng, R. X. Wang, *Polyhedron* **1997**, *16*, 2991.

[30] X. H. Bu, M. Du, Z. L. Shang, L. Zhang, Q. H. Zhao, R. H. Zhang, M. Shionoya, *Eur. J. Inorg. Chem.* **2001**, 1551.

[31] S. J. Brown, X. Tao, T. A. Wark, D. W. Stephan, P. K. Mascharak, *Inorg. Chem.* **1988**, *27*, 1581.

[32] R. Acevedo-Vhavez, M. E. Costas, R. Escuredo, *Inorg. Chem.* **1996**, *35*, 7430.

[33] G. A. v. Albada, O. Roubeau, H. K. P. Gamez, A. L. Spek, J. Reedijk, *Inorg. Chim. Acta* **2004**, *357*, 4522.

[34] R. Cortes, L. Lezama, J. I. R. Larramendi, G. Madariaga, J. L. Mesa, F. J. Zuniga, T. Rojo, *Inorg. Chem.* **1995**, *34*, 778.

[35] A. Bencini, D. Gatteschi, C. Zanchini, *J. Am. Chem. Soc.* **1980**, *102*, 5234.

[36] G. A. v. Albada, W. J. J. Smeeth, A. L. Spek, J. Reedijk, *Inorg. Chim. Acta* **2000**, *299*, 35.

[37] B. J. Hathaway in *Comprehensive Coordination Chemistry, Vol. 5* (Eds.: G. Wilkinson, R. D. Gillard, J. McCleverty), Pergamon, Oxford, **1987**.

[38] H. Yokoi, A. W. Addison, *Inorg. Chem.* **1977**, *16*, 1341.

[39] A. V. Malkov, I. R. Baxendale, M. Bella, V. Langer, J. Fawcett, D. R. Russel, D. J. Mansfield, M. Valko, P. Kocovsky, *Organometallics* **2001**, *20*, 673.

[40] T. S. Ertel, H. Bertagnolli, S. Hückmann, U. Kolb, D. Peter, *Appl. Spectrosc.* **1992**, *46*, 690.

[41] M. Newville, P. Livins, Y. Yakoby, J. J. Rehr, E. A. Stern, *Phys. Rev. B* **1993**, *47*, 14126.

[42] S. J. Gurman, N. Binsted, I. Ross, *J. Phys. C* **1986**, *19*, 1845.

[43] G. Gescheidt, *Rev. Sci. Instrum.* **1994**, *65*, 2145.

[44] S. Stoll, A. Schweiger, *J. Magn. Reson.* **2006**, *178*, 42–55.

[45] SimfFonia, Version 1.25, Bruker Biospin, Rheinstetten, Germany **1996**.

[46] Taken from: Marc Martin, Dissertation, RWTH Aachen, **2002**.